International Journal of Environmental Science and Technology (2025) 22:15273–15288
https://doi.org/10.1007/s13762-025-06623-x

ORIGINAL PAPER

Using citric acid production waste as a new material for an air humidity sensor

T. B. Nikulicheva[1] · V. S. Zakhvalinsky[1] · V. V. Vyazmin[1] · I. S. Nikulin[1] · O. A. Telpova[1] · V. B. Nikulichev[2]

Received: 18 February 2025 / Revised: 6 May 2025 / Accepted: 16 June 2025 / Published online: 12 July 2025

Abstract

Currently, one of the solutions for recycling by-products of technological processes that accumulate as production waste is their use as functional materials of electronics. The main objective of our study was to determine the sensitivity of samples to air humidity using impedance spectroscopy. The properties of samples obtained by uniaxial and isostatic pressing methods from calcium sulfate hemihydrate and calcium sulfate dihydrate were studied. The impedance of the samples was studied as a function of relative air humidity at different frequencies. Cyclic dependencies of the complex resistance response were observed when relative humidity varied in the range 40 to 80% within the frequency range from 200 Hz to 1 MHz. Based on the results of the studies, a conclusion was made about the possibility of practical application of waste from the technological process of producing food citric acid, citrogypsum, as a source for obtaining a new material for an air humidity sensor.

Keywords Citrogypsum · Humidity sensor · Resistive humidity sensor · Impedance spectroscopy

Introduction

Intelligent electronic systems are involved in all aspects of modern human life, they improve the quality of life and help control health. At the same time, the processes of obtaining materials for the manufacture of electronic devices, including those improving technological processes in industry and agriculture, are a source of increasing waste and put a burden on the environment and pose a threat to human health (Patrusheva et al. 2018). The growing amount of household and industrial process waste has a negative impact on the environment worldwide (Tao et al. 2021). Part of the solution to the waste problem is to use naturally occurring materials that do not have a strong impact on the environment. At the same time, the effect is enhanced if these materials are waste from technological processes and are utilized in the production of electronic components, such as air humidity sensors.

Air humidity sensors differ in their physical principles of operation and design (Nikulicheva et al. 2023a; Kang and Wise 2000; Vooka and George 2014). A number of materials are known that are used to manufacture air humidity sensors (Wang et al. 2013; Li and Yang 2002; Adhikari and Majumdar 2004). An essential condition for using new materials is maintaining functional characteristics and reducing the cost of sensors when using waste from technological production; these conditions must be combined with reducing the environmental burden on the environment. Waste from various industrial productions for use as sensor material requires additional purification or modification, since they must react to air humidity by changing at least one of such parameters as resistance, capacity, pH, or color of the material. Regardless of the design and operating principle, the sensors currently in use either repeatedly and quickly return to their original state before the measurement cycle, or smoothly and reversibly change parameters with increases and decreases in air humidity. Therefore, the search for new materials used in humidity sensors is relevant due to their widespread use in everyday life (Hossein-Babaei and Shabani 2014), in the food industry (Bridgeman et al. 2014), in agriculture (Matko and Donlagic 1996) and in medicine (Selyanchyn et al. 2015).

Compounds based on calcium sulfate are insulators, which is an advantage when used as structural materials

Editorial responsibility: Samareh Mirkia.

✉ T. B. Nikulicheva
t_nikulicheva@inbox.ru

[1] Belgorod National Research University, 85, Pobedy St., Belgorod, Russia 308015

[2] Belgorod State Technological University Named After V.G. Shukhov, 46, Kostyukova St., Belgorod, Russia 308012

primarily in the construction and chemical industries. Obtaining conductive compounds based on chemically modified calcium sulfate with different electrical conductivity values from the initial insulator state to the highly conductive state of a solid electrolyte allows finding new areas of application for such compounds as functional ones, for example, when creating humidity sensors.

The process of modifying the electrical properties of gypsum is possible using acids and salts (Abe et al. 2006, 2007; Suzuki et al. 2011; Nikulicheva et al. 2023b, 2024), which leads to a partial replacement of the cationic group in the compounds being processed with a proton of the acid or salt, thus forming a solid electrolyte with proton conductivity.

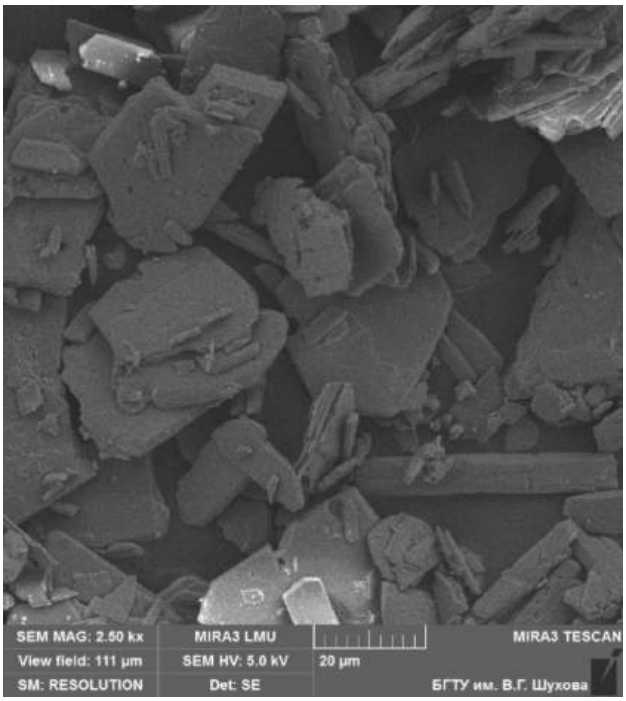

Fig. 1 Surface morphology of original citrogypsum particles

According to the results presented in Abe et al. (2006); Abe et al. 2007; Suzuki et al. 2011), treating gypsum in phosphoric acid leads to the appearance of proton conductivity in the treated material. In (Nikulicheva et al. 2023b, 2024), the modification of electrical properties with copper sulfate at room temperature was considered. The appearance of proton conductivity due to chemical modification with acids and salts is associated with the presence and interaction with a chain network of hydrogen bonds located along the c axis in calcium sulfate hemihydrate and a flat network of hydrogen bonds formed between the (020) planes in calcium sulfate dihydrate (Xin et al. 2015). The existence of chains of hydrogen bonds and water channels affects the electrical properties of calcium sulfate.

This article is devoted to the use of a waste product of the technological process of production of food citric acid, citrogypsum, (Sirimahasal et al. 2019; Alfimova et al. 2020) as a potential material for humidity sensors. A comparison of the properties of samples of calcium sulfate hemihydrate and calcium sulfate dihydrate obtained by the method of uniaxial pressing in a mold and by the method of isostatic pressing is carried out. Competitive advantages of sensors made of citrogypsum are low cost, environmentally friendly raw materials, and technologically advanced manufacturing of the moisture-absorbing layer from citrogypsum. According to the World Health Organization (WHO) classification, citrogypsum has the Class III (slightly hazardous) hazard class.

Table 3 Plan matrix for the experiment

		Material	
Pressing method	Uniaxial	$CaSO_4 \cdot 2H_2O$	
			$CaSO_4 \cdot 0.5H_2O$
	Isostatic	$CaSO_4 \cdot 2H_2O$	
			$CaSO_4 \cdot 0.5H_2O$

Table 1 Chemical analysis of original citrogypsum

Oxide content (wt%)									
CaO	SiO_2	Al_2O_3	MgO	SO_3	Na_2O	K_2O	Fe_2O_3/FeO	SrO	P_2O_5
43.36	0.54	0.13	0.06	55.47	0.04	0.03	0.15	0.14	0.08

Table 2 Grain composition and fineness modulus of original citrogypsum

Name of residue	Residues, % by weight, on sieves								Fineness modulus
Sieve Number	5	2.5	1.25	0.63	0.315	0.16	0.08	< 0.08	2.15
Particular (g)	0.9	4.1	159.8	24.7	31.8	7.1	2.1	0.4	
Particular (wt.%)	16.5	8.9	7.4	10.5	9.2	8.9	38.56	0	
Full (wt.%)	16.5	25.4	32.8	40.3	52.5	61.4	100	100	

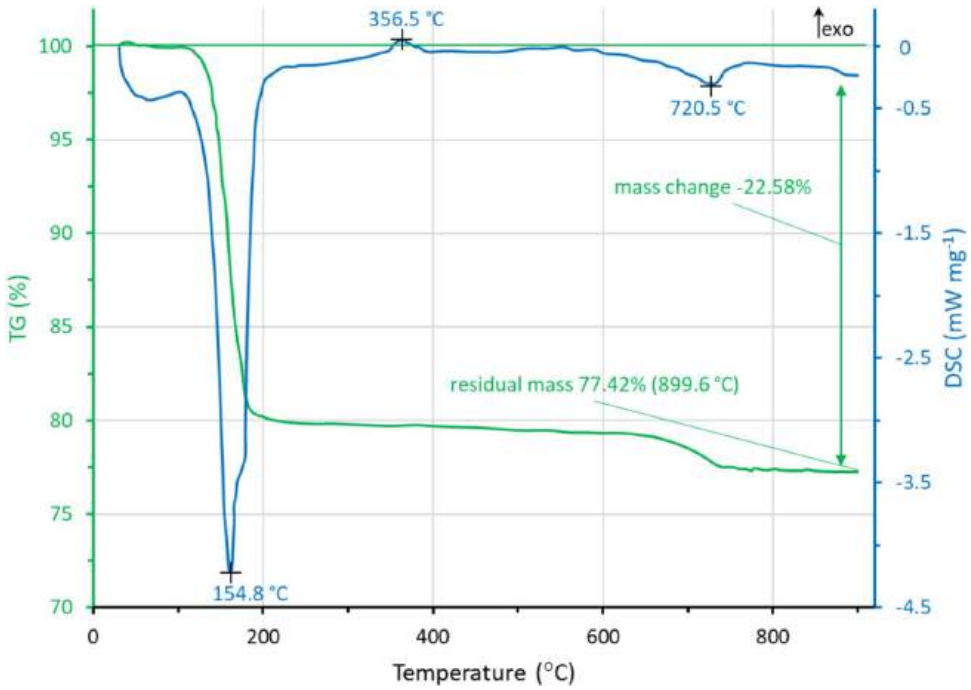

Fig. 2 Thermogram of the original citrogypsum

This research was conducted at the Laboratory of Advanced Materials and Technologies, Belgorod National Research University, from July 2024 to October 2024.

Materials and methods

Technology of obtaining samples and research methods.

The raw material used in this work was waste from the biochemical production of citric acid, citrogypsum, Belgorod, Russia.

The surface morphology analysis of citrogypsum particles was carried out using a TESCAN MIRA 3 LMU high-resolution scanning electron microscope, including an X-MAX 50 Oxford Instruments NanoAnalysis energy dispersive spectrometer. Analysis of the morphology of citrogypsum particles showed that this raw material is mainly represented by large plate-shaped particles with a developed surface, against the background of which an insignificant number of columnar particles are visible (Fig. 1). With multiple magnification, it is evident that the particles have a highly developed porous surface structure, the formation of which is due to technological features, as well as the impact of natural factors.

The chemical composition of the studied citrogypsum was determined by X-ray fluorescence analysis (XRF) using the WorkStation ARL 9900 X-ray workstation (Thermo Scientific, USA), using the radiation of the Co anode. According to the given chemical composition (Table 1), the used citrogypsum is mainly represented by CaO and SO_3 oxides, which together provide ≈ 99%. In other words, citrogypsum consists of ≈ 99% $CaSO_4$ with minor impurities of iron, silicon and aluminum oxides, which together do not exceed 1%.

To quantitatively assess the granulometry of the waste, they were first sifted by fractions. Based on the sifting results, the grain size composition and fineness modulus of the material under study were obtained, which are presented in Table 2. It was found that ≈ 40% of the citrogypsum particles are in the fraction area of less than 0.16 mm.

Table 4 Parameters of samples: *a*—length, *b*—width, *h*—height, *m*—mass

	a (mm)	*b* (mm)	*h* (mm)	*m* (g)
$CaSO_4 \cdot 2H_2O$, uniaxial pressing (sample I)	7.2	8.5	2.2	0.241
$CaSO_4 \cdot 0.5H_2O$, uniaxial pressing (sample II)	7.2	8.5	2.2	0.210
$CaSO_4 \cdot 2H_2O$, isostatic pressing (sample III)	7.2	9.2	2.2	0.246
$CaSO_4 \cdot 0.5H_2O$, isostatic pressing (sample IV)	7.2	9.2	2.2	0.332

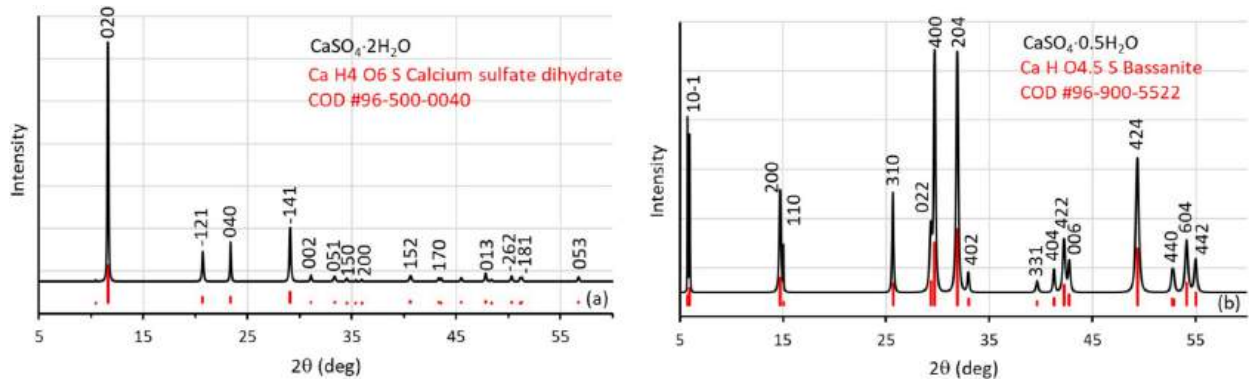

Fig. 3 X-ray spectrum of **a** $CaSO_4 \cdot 2H_2O$ and **b** $CaSO_4 \cdot 0.5H_2O$ and peak positions from the COD database (red lines)

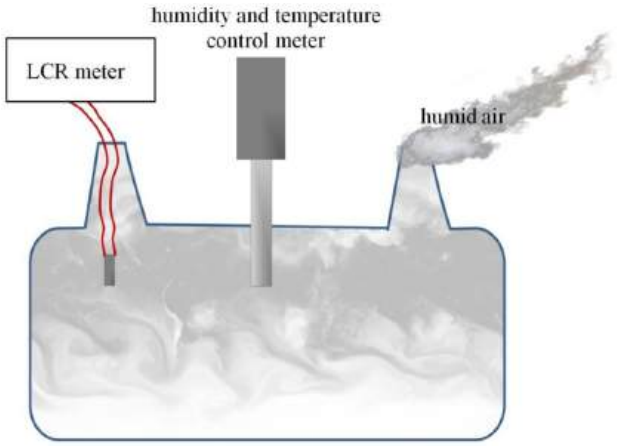

Fig. 4 Schematic representation of the test humidity chamber at the time of measurements

The remaining 60% are uniformly distributed in the fraction range of 0.1–5 mm.

After that, a granulometric analysis of the citrogypsum by the laser granulometry method using an ANALYSETTE 22 NanoTec plus laser particle analyzer (Fritsch, Germany) was carried out, which provides an estimate of the grain size in the range from 0.2 to 600 µm for 40 fractions of the material under study, presenting the data as a percentage. According to the results of the granulometric analysis, citrogypsum has 2 size peaks with the main ranges of the size distribution from 20 to 200 µm and from 500 to 700 µm.

As noted in Table 1, citrogypsum is completely consistent with its natural analogue and consists of 99% calcium sulfate $CaSO_4$. This is what sets citrogypsum apart from its closest analogue, phosphogypsum, which is a waste product of sulfuric acid production of mineral fertilizers, formed during the sulfuric acid processing of natural apatites and phosphorites into phosphoric acid, double superphosphate, ammonium phosphate precipitate and other concentrated fertilizers. Due to the production technology, phosphogypsum contains impurities of P_2O_5 (0.7–3.02% P_2O_5 (Gu and Chen 2020; Huang et al. 2019)), as well as As, Pb, Cd, Mn, Fe, Zn, Cu, Co, La, Ni, Cr, Se, Hg and F. The presence of these impurities will certainly affect the intragranular and intergranular conductivity, conductivity mechanisms, permittivity, capacitance, impedance and frequency range of moisture sensitivity. Moreover, it is very difficult to control the repeatability of electrical properties of several samples on this raw material, since the amount of impurities also strongly depends on the source of the raw material, which is not observed for citrogypsum taken from different sources.

In Nikulicheva et al. (2023b) we already described the physicochemical properties of citrogypsum obtained from waste from an industrial technological process, the production and the possibility of practical application of a new composite material $(CaSO_4 \cdot 2H_2O)_{0.975}$-$(CuSO_4 \cdot 5H_2O)_{0.025}$ in air humidity sensors. In this work, two types of material and two types of pressing were used for research, in accordance with the plan matrix specified in Table 3.

To obtain a sample of calcium sulfate dihydrate, citrogypsum was taken, in which, according to the results of differential scanning calorimetry (DSC) and thermogravimetric analysis (TG) (Fig. 2), the ratio of calcium sulfate dihydrate ($CaSO_4 \cdot 2H_2O$) to calcium sulfate hemihydrate ($CaSO_4 \cdot 0.5H_2O$) was 13:1, respectively.

To obtain calcium sulfate dihydrate, 100 g of the original citrogypsum were sifted through a 100 µm sieve. Then, more than enough citrogypsum was dissolved in distilled water at a rate of 250 ml H_2O per 10 g of citrogypsum. The undissolved precipitate was filtered and dried in a drying cabinet at a temperature of 60 °C for 2 h.

Calcium sulfate hemihydrate was obtained from 100 g of calcium sulfate dihydrate, which was fired in a furnace at a temperature of 150 °C for 4 h, followed by reduction at room temperature for 24 h.

Uniaxial pressing was performed on an Universal Testing Machine (Instron Electromechanical Testing systems) Model 3369.

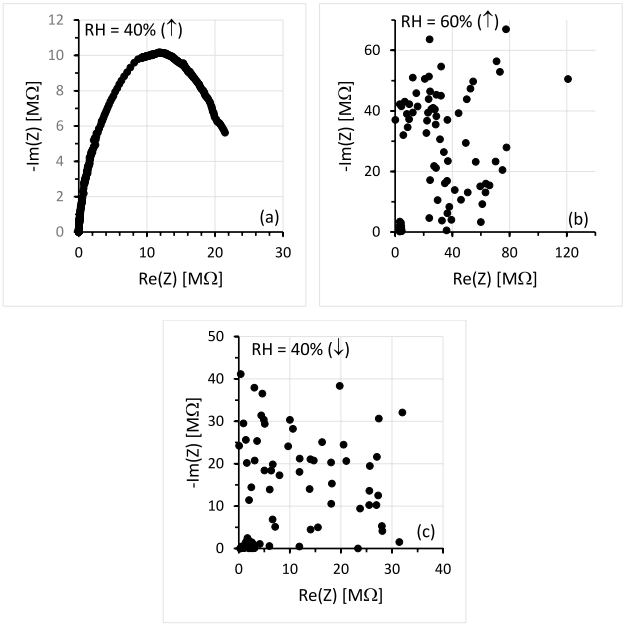

Fig. 5 Impedance diagram of $CaSO_4 \cdot 2H_2O$ samples obtained by uniaxial pressing (I) at RH = 40% (**a**), (**c**) and RH = 60% (**b**). The directions of the arrows indicate that the humidity in the test chamber increases (↑) or decreases (↓)

Samples of calcium sulfate dihydrate were obtained using the semi-dry uniaxial pressing method. For this purpose, distilled water was added to $CaSO_4 \cdot 2H_2O$ at a rate of 2 ml H_2O per 10 g of calcium sulfate dihydrate and mixed well until a homogeneous semi-dry mixture was obtained. The resulting mixture was pressed at a pressure of 180 MPa with an exposure at a given pressure of 120 s. After removing the sample from the press mold, the sample was dried at 40 °C for 2 h to remove excess moisture from the sample.

To obtain samples from calcium sulfate hemihydrate, the samples of $CaSO_4 \cdot 2H_2O$ obtained by the semi-dry uniaxial pressing method described above, removed from the press mold, were dried at a temperature of 150 °C for 4 h, followed by recovery at room temperature for 24 h.

Cold isostatic pressing was performed on an EPSI isostatic press in a special silicone mold. Samples of calcium sulfate dihydrate and calcium sulfate hemihydrate were pressed at a pressure of 1800 atm in a silicone mold (180 MPa) with an exposure at a given pressure of 120 s.

Then, samples of the required sizes (Table 4) were prepared from the pressed samples by grinding, on which a study of the dielectric properties was carried out at a relative humidity (RH) in the range of 40–80% by impedance spectroscopy.

X-ray diffraction analysis of the obtained samples was carried out on a Rigaku SmartLab diffractometer with Bragg–Brentano focusing, using CuKα radiation at a voltage of 60 kV and a current of 60 mA. Surveys were carried out in the 2θ angle range from 10 to 60°. The scanning step was 0.02°, the exposure time was 20 s. According to the X-ray diffraction data, it is possible to experimentally determine the size of the coherent scattering region (CSR) based on the data on the broadening of diffraction reflections in order to assess the microdistortions of the crystal lattice. The average CSR size was $d = 57.2 \pm 2.4$ nm for $CaSO_4 \cdot 2H_2O$ and $d = 32.8 \pm 1.3$ nm for $CaSO_4 \cdot 0.5H_2O$. Figure 3 shows the X-ray spectrum of the obtained samples from $CaSO_4 \cdot 2H_2O$ and $CaSO_4 \cdot 0.5H_2O$.

Electrical contacts were obtained by sputtering silver onto the opposite faces of samples I–IV (Table 4) using the RF magnetron sputtering method on a VN-2000 setup. As a result, Ag/($CaSO_4 \cdot 0.5H_2O$)/Ag and Ag/($CaSO_4 \cdot 2H_2O$)/Ag samples were obtained, to the contact pads of which

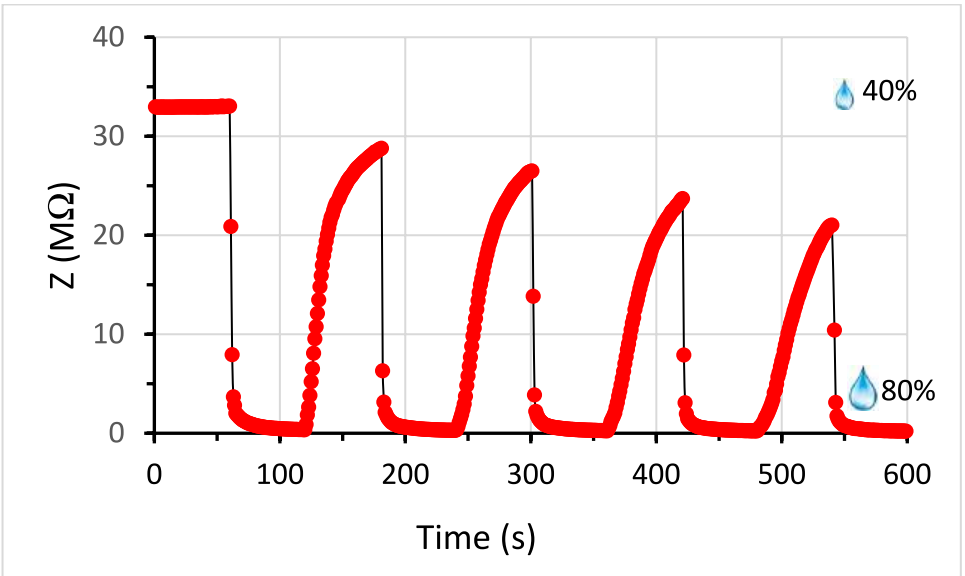

Fig. 6 Impedance switching cycles of $CaSO_4 \cdot 2H_2O$ samples obtained by uniaxial pressing (I) at RH = 40–80% at a frequency of 1 kHz and a voltage of 1 V

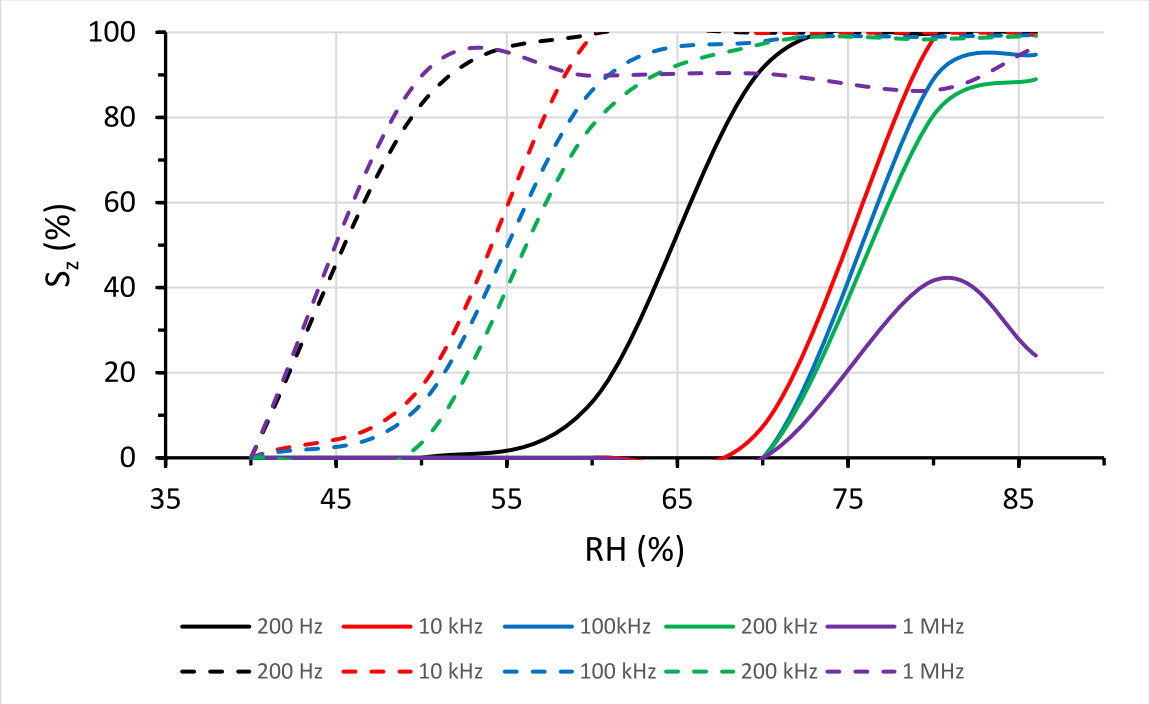

Fig. 7 Impedance sensitivity of a $CaSO_4 \cdot 2H_2O$ sample obtained by uniaxial pressing (I) to humidity with increasing and decreasing humidity at frequencies of 200 Hz, 10 kHz, 100 kHz, 200 kHz, 1 MHz. The directions of the arrows indicate that the humidity in the test chamber increases (↑) or decreases (↓)

measuring probes were attached with silver conductive paste.

The samples were tested in a specially designed humidity chamber, which is a closed chamber with inlet and outlet valves for gas. An UN-232 nebulizer was used to create humidity in the chamber. To reduce humidity in the chamber, steam was blown out with dry air. Measurements were carried out at a constant temperature of 28 °C and a relative humidity range 40 to 80% (Fig. 4).

Research methodology

The impedance spectroscopy method involves applying a small-amplitude sinusoidal excitation signal to the system under study and studying the resulting output response signal. The experiment involved applying alternating electric current to the samples and measuring the frequency dependence of the active R and reactive X components of the complex impedance $Z = R + jX$, where j is the imaginary unit. The capacitance, conductivity and impedance were measured using an LCR meter (AKTAKOM Model AM-3026) with an alternating signal amplitude of 1 V. Humidity and temperature in the chamber were monitored using a humidity meter (AKTAKOM Model ATE-5035).

The suitability of samples I–IV for operation as humidity sensors was analyzed based on the measured impedance frequency dependences in the range from 200 Hz to 1 MHz and impedance switching cycles in the relative humidity range from 40 to 80%. The impedance spectroscopy results for the $Ag/(CaSO_4 \cdot 0.5H_2O)/Ag$ and $Ag/(CaSO_4 \cdot 2H_2O)/Ag$ samples obtained by uniaxial and isostatic pressing differ from each other. The choice of pressing method affects the sensitivity of $CaSO_4 \cdot 0.5H_2O$ and $CaSO_4 \cdot 2H_2O$ to air humidity.

Results and discussion

Frequency dependence of impedance of a sample of calcium sulfate dihydrate $CaSO_4 \cdot 2H_2O$ obtained by uniaxial pressing at 180 MPa

The study of samples (I) showed that during the initial measurement of impedance at an initial RH = 40%, a hodograph is observed (Fig. 5a).

A further increase in humidity, for example, to RH = 60%, leads to the absence of the hodograph (Fig. 5b). When the humidity decreases to RH = 40% (Fig. 5c), the hodograph is not restored. This indicates that the adsorption water present

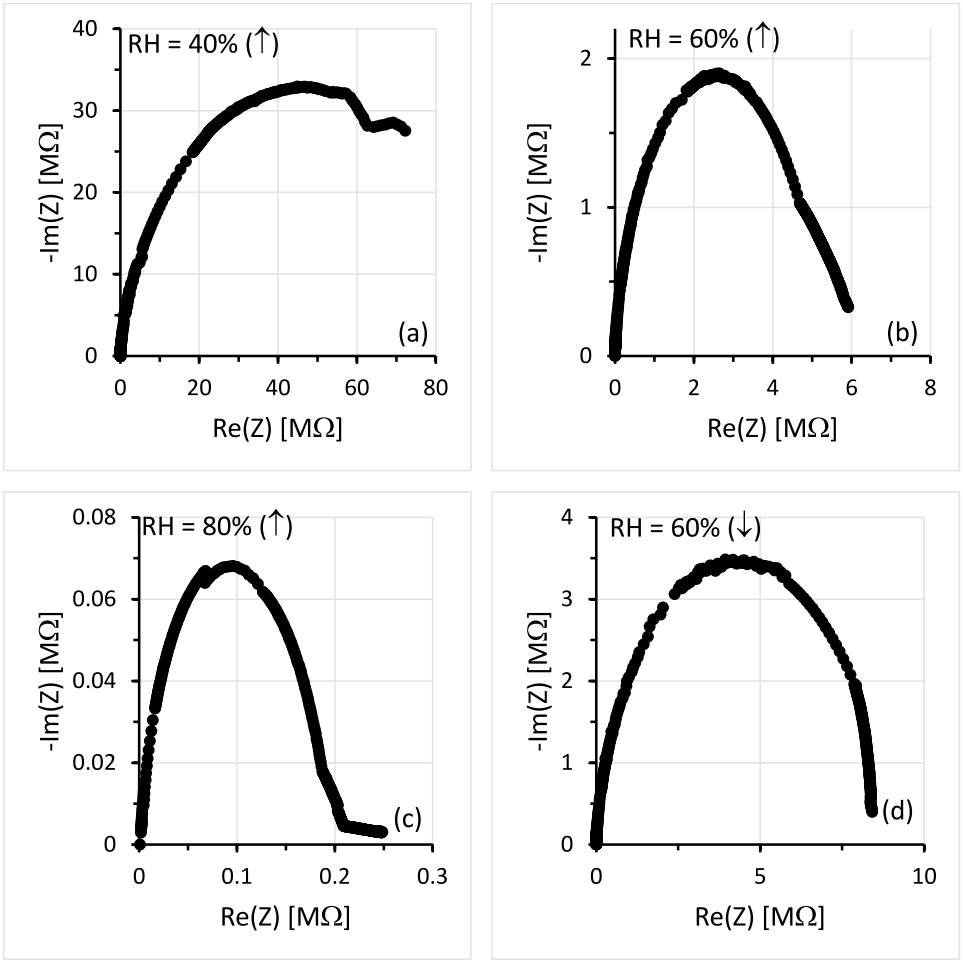

Fig. 8 Impedance diagram of $CaSO_4 \cdot 0.5H_2O$ samples obtained by uniaxial pressing (II) at RH = 40% (**a**), RH = 60% (**b**), (**d**) and RH = 80% (**c**). The directions of the arrows indicate that the humidity in the test chamber increases (↑) or decreases (↓)

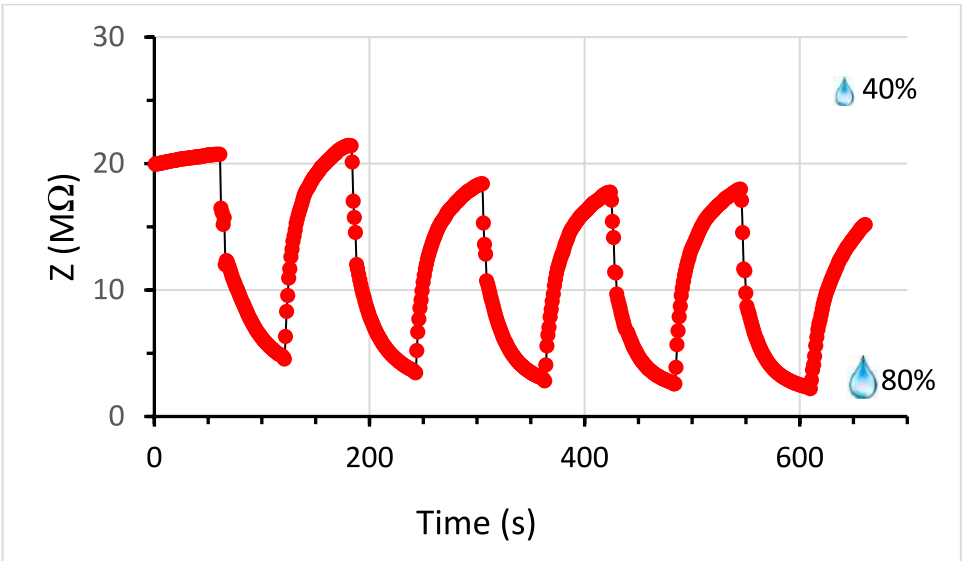

Fig. 9 Impedance switching cycles of $CaSO_4 \cdot 0.5H_2O$ samples obtained by uniaxial pressing (II) in the range of relative humidity of 40–80% at a frequency of 1 kHz and a voltage of 1 V

in the sample due to the increase in humidity is bound and can only be removed by drying.

The results of the study of the cyclicity of the complex impedance response *Z* with a change in relative air humidity from 40 to 80% are shown in Fig. 6.

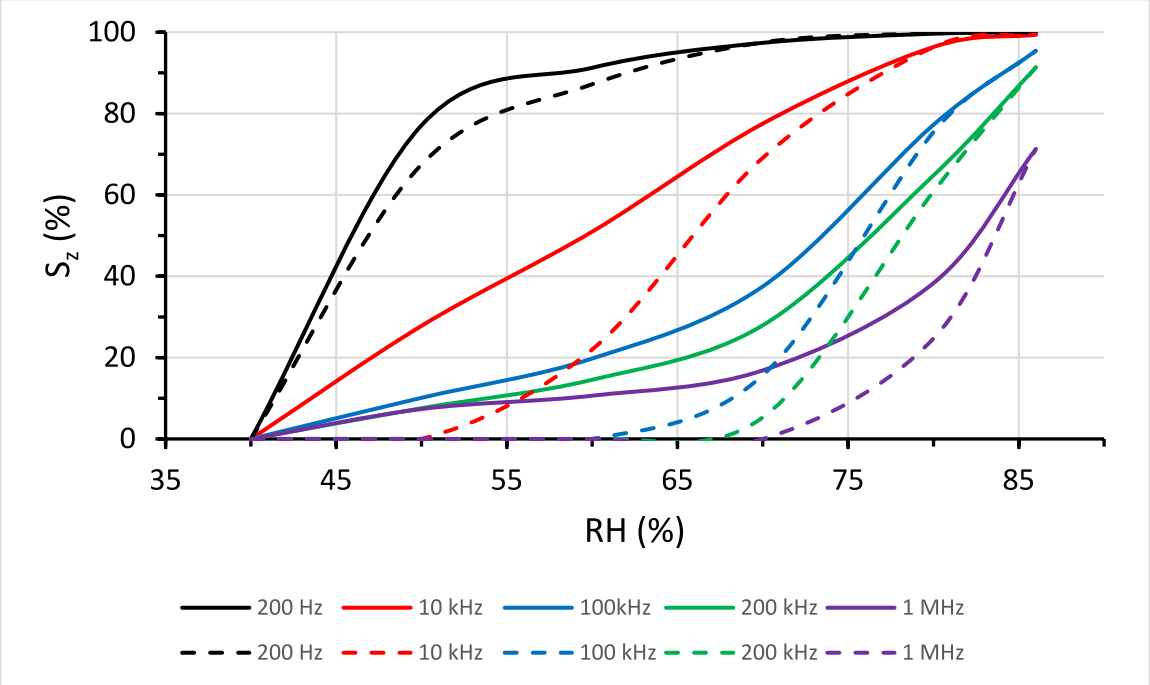

Fig. 10 Impedance sensitivity of the $CaSO_4 \cdot 0.5H_2O$ sample obtained by uniaxial pressing (II) to humidity with increasing and decreasing humidity at frequencies of 200 Hz, 10 kHz, 100 kHz, 200 kHz, 1 MHz. The directions of the arrows indicate that the humidity in the test chamber increases (↑) or decreases (↓)

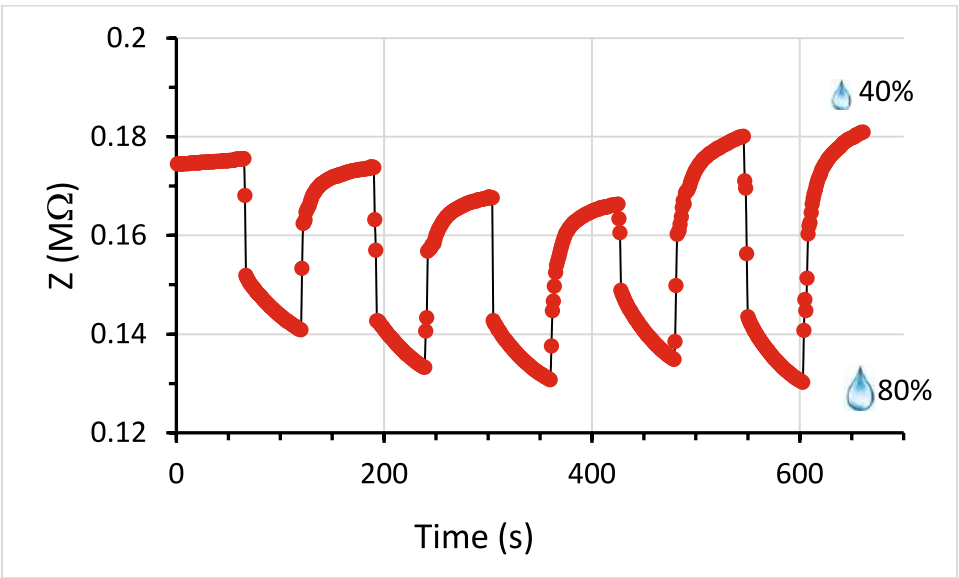

Fig. 11 Impedance switching cycles of $CaSO_4 \cdot 0.5H_2O$ samples obtained by uniaxial pressing (II) in the range of relative humidity of 40–80% at a frequency of 200 kHz and a voltage of 1 V

The sample was placed in turn in the test chamber at RH = 80%, and then in the reference chamber, in which a constant air temperature of 28 °C and a relative humidity of 40% were maintained. The time spent in the test chamber and the time spent in the reference chamber was 60 s. The cycle was repeated 5 times. The complex impedance Z in the first cycle changed from 32 to 1 MOhm, with the repetition of cycles, the interval in the 5th cycle was from 21 to 1 MOhm. This indicates that this sample is not suitable as a material for a cyclic humidity sensor without preliminary drying before starting the measurements.

To determine the sensitivity of the sample impedance to air humidity, formula (1) was used:

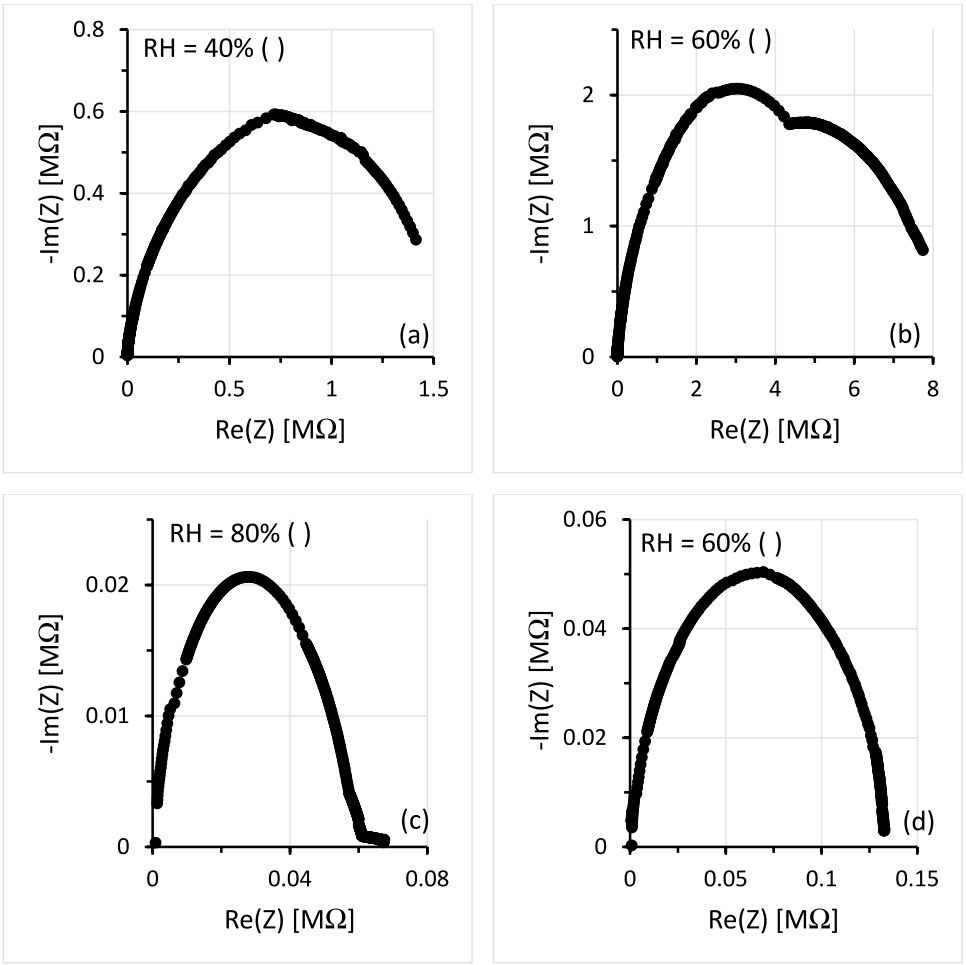

Fig. 12 Impedance diagram of $CaSO_4 \cdot 2H_2O$ samples obtained by isostatic pressing (III) at RH = 40% (**a**), RH = 60% (**b**), (**d**) and RH = 80% (**c**). The directions of the arrows indicate that the humidity in the test chamber increases (↑) or decreases (↓)

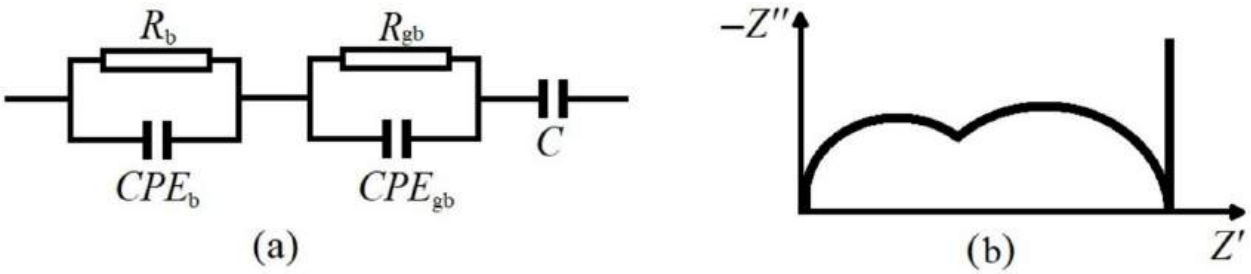

Fig. 13 Equivalent circuit of a cell with two parallel strings (**a**) and impedance (**b**) for partially overlapping circles

$$S_z = \frac{Z[40] - Z[RH]}{Z[40]} \times 100\% \quad (1)$$

where $Z[40]$ is the complex impedance at a relative humidity of 40%, $Z[RH]$ is the complex impedance at the studied air humidity.

The sensitivity of the sample impedance (I) to air humidity was determined with increasing and decreasing humidity in the frequency range from 200 Hz to 1 MHz (Fig. 7).

When humidity decreases and increases, hysteresis is observed, the nature of which changes depending on the signal frequency, and at a frequency of 1 MHz the hysteresis shape is disrupted. The correct and closed shape of the sample hysteresis is observed at frequencies up to 10 kHz.

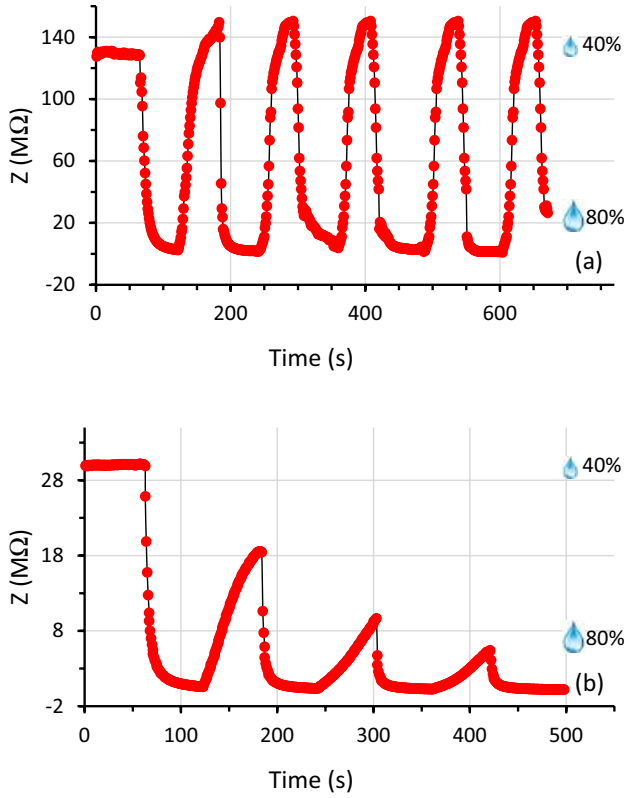

Fig. 14 Impedance switching cycles of $CaSO_4 \cdot 2H_2O$ samples obtained by isostatic pressing (III) at RH = 40–80% at a voltage of 1 V at frequencies of 200 Hz (**a**) and 1 kHz (**b**)

Frequency dependence of impedance of a sample of calcium sulfate hemihydrate $CaSO_4 \cdot 0.5H_2O$ obtained by uniaxial pressing at 180 MPa

The study of samples (II) showed that the hodographs obtained at high humidity (Fig. 8) represent an arc of varying degrees of closure; with increasing humidity, the closure increases, and the impedance changes with increasing humidity. With decreasing humidity, the degree of closure of the hodograph becomes more pronounced (Fig. 8b, d).

Figure 9 shows the results of measuring the cyclicity of the response of the complex impedance *Z* with a change in relative air humidity from 40 to 80% at a frequency of 1 kHz. The method for measuring the cyclicity is similar to that for measuring the cyclicity of the response of the complex impedance of the sample (I).

A decrease in the complex impedance from 21 to 4 MOhm is observed in the first cycle with an increase in RH = 40 to 80%, the impedance is maintained in the second cycle and decreased to 18 MOhm in the third recovery cycle (Fig. 9). In subsequent cycles, the complex impedance is maintained. It can be assumed that sample (II) can be used as a material for continuous monitoring of air humidity, but several initial cycles are required to stabilize the mode. The sensitivity of the impedance of sample (II) to air humidity was also studied in accordance with formula (1) in the frequency range from 200 Hz to 1 MHz (Fig. 10).

When humidity decreases and increases, hysteresis is also observed, changing with the signal frequency. At a frequency of 200 Hz, the hysteresis loop has a closed shape over the entire range of relative humidity and a minimum area. With an increase in frequency, the hysteresis loop increases its area and changes shape when the RH changes from 40 to 80%, which correlates with a violation of the cyclic reproducibility of the response and the impedance value *Z* at high frequencies (Fig. 11).

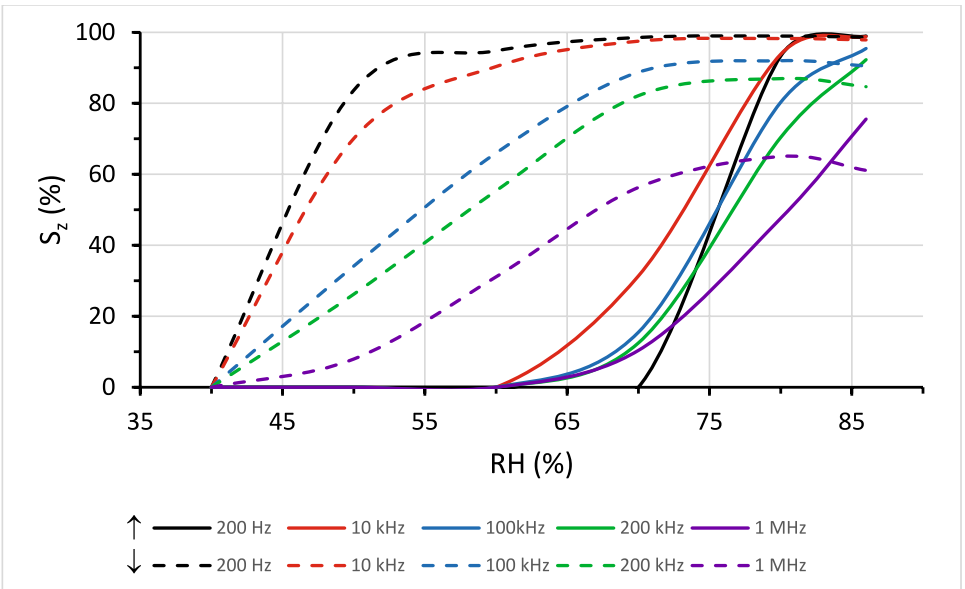

Fig. 15 Impedance sensitivity of the $CaSO_4 \cdot 2H_2O$ sample obtained by isostatic pressing (III) to humidity with increasing and decreasing humidity at frequencies of 200 Hz, 10 kHz, 100 kHz, 200 kHz, 1 MHz. The directions of the arrows show that the humidity in the test chamber increases (↑) or decreases (↓)

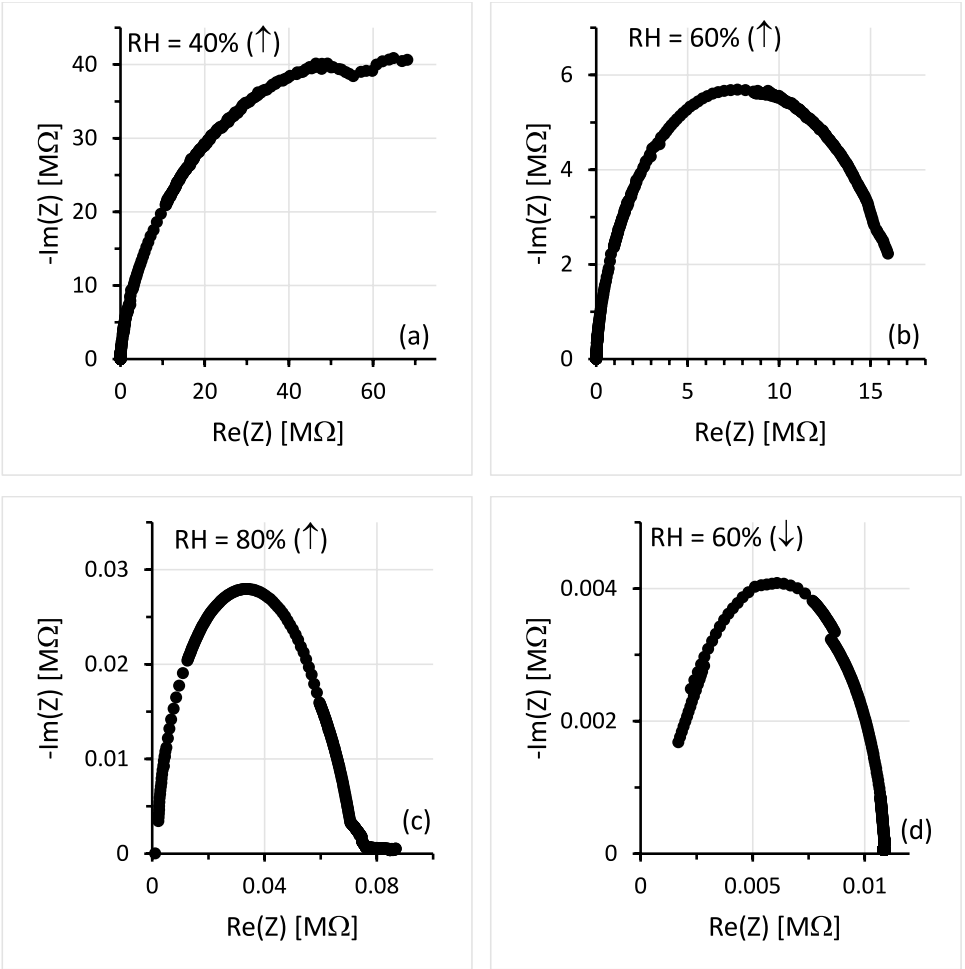

Fig. 16 Impedance diagram of $CaSO_4 \cdot 0.5H_2O$ samples obtained by isostatic pressing (IV) at RH = 40% (**a**), RH = 60% (**b**), (**d**) and RH = 80% (**c**). The directions of the arrows indicate that the humidity in the test chamber increases (↑) or decreases (↓)

Frequency dependence of impedance of a sample of calcium sulfate dihydrate $CaSO_4 \cdot 2H_2O$ obtained by isostatic pressing at 180 MPa

The study of samples (III) is presented in Fig. 12.

As follows from Fig. 12, as the humidity increases, the hodograph forms partially overlapping circles, the contribution of which to the frequency dependence of the impedance changes. If the complex impedance is due to grain conductivity, i.e., is characterized by the intrinsic capacitance of the grains, then the equivalent circuit can be as shown in Fig. 13, a. Here, R_g is the resistance of a single grain, R_{gb} is the resistance of grain boundaries, C is the capacitance characteristic of solid-state systems, described by the formula of a flat capacitor, the constant phase element CPE_g is the capacitive parameter of the grain, and the constant phase element CPE_{gb} is the capacitive parameter of the grain boundaries. In case of series connection of two parallel circuits from a capacitance and a resistance, either partially overlapping or non-overlapping circles can be obtained. In case the time constants τ for two RC circuits differ significantly, the circles do not overlap. If τ_1 and τ_2 differ insignificantly, overlapping of semicircles is observed (Fig. 13b). Evolution of overlapping of semicircles on frequency dependences of impedance of $CaSO_4 \cdot 2H_2O$ samples obtained by isostatic pressing (III) depending on humidity is observed in Fig. 12b. As humidity increases, the closure of the first semicircle increases and a low-frequency line appears, corresponding to the processes occurring on the electrodes (Fig. 12c). Hodographs are observed both when shooting a sequence of dependences in the direction of increasing and in the direction of decreasing humidity (Fig. 12d).

To demonstrate the practical application possibilities of samples (III) as an air humidity sensor, the response and impedance recovery cycles were measured when the relative air humidity changed from 40 to 80% at different frequencies: 200 Hz and 1 kHz (Fig. 14).

The method for measuring the cyclicity corresponds to the measurement of the cyclicity of the complex impedance response of sample (I), described above.

As a result of increasing the air humidity from 40 to 80%, the impedance measured at a frequency of 200 Hz decreased in the first cycle from 130 to 5 MOhm. From the second cycle onwards, the difference stabilized and changed

from 150 to 5 MOhm, and after moving the sample from the test chamber to the reference chamber, the sample was restored within 1 s (Fig. 14a). With an increase in frequency to 1 kHz, the impedance recovery during cyclic changes in humidity is disrupted (Fig. 14b).

To determine the sensitivity of the sample impedance to air humidity, in the frequency range from 200 Hz to 1 MHz formula (1) was used (Fig. 15).

It follows from Fig. 15 that if the frequency exceeds a certain threshold value (100 kHz), the dependence of the impedance sensitivity on the relative humidity becomes hysteretic and has an asymmetrical character. At a frequency of 200 Hz, the hysteresis loop has a regular closed shape over the entire range of relative humidity. With an increase in frequency, the hysteresis loop opens and does not cover the entire measurement range, which correlates with a violation of the cyclic reproducibility of the impedance when the relative humidity of the air changes from 40 to 80% at high frequencies (Fig. 14b).

Frequency dependence of impedance of a sample of calcium sulfate hemihydrate $CaSO_4 \cdot 0.5H_2O$ obtained by isostatic pressing at 180 MPa

The study of samples (IV) is presented in Fig. 16. The hodographs obtained at low humidity (Fig. 16a, b, d) represent an arc of varying degrees of closure, with elements of the second semicircle at low frequency. As humidity increases, the closure of the first semicircle increases and a low-frequency line appears, corresponding to the processes occurring on the electrodes (Fig. 16c).

As follows from the results of the study of the complex impedance with a change in the relative humidity of the air from 40 to 80% of the samples (IV), at frequencies of 200 Hz and 1 kHz (Fig. 17), the reproducibility of the impedance response cycles from the humidity of the samples (IV) is comparable to the cyclicity of the impedance switching of the samples (II) (Figs. 9, 11). When placing the sample (IV) in the test chamber with a relative humidity of 80%, as follows from Fig. 17a, at a frequency of 200 Hz, the impedance decreases from 36 to 5 MOhm in the first cycle. In subsequent cycles, impedance recovery is observed in a very short period of time when moving the sample to the reference chamber with a relative humidity of 40%. From the third cycle and further, when placing the sample in the test chamber, reproducibility of the cyclicity is observed even at high humidity. At a frequency of 1 kHz, a violation of the cyclicity of the impedance response and a tendency for a slight increase in impedance in each subsequent recovery cycle are observed (Fig. 17b).

We measured the impedance switching parameters for our samples (Table 5) are comparable with other materials

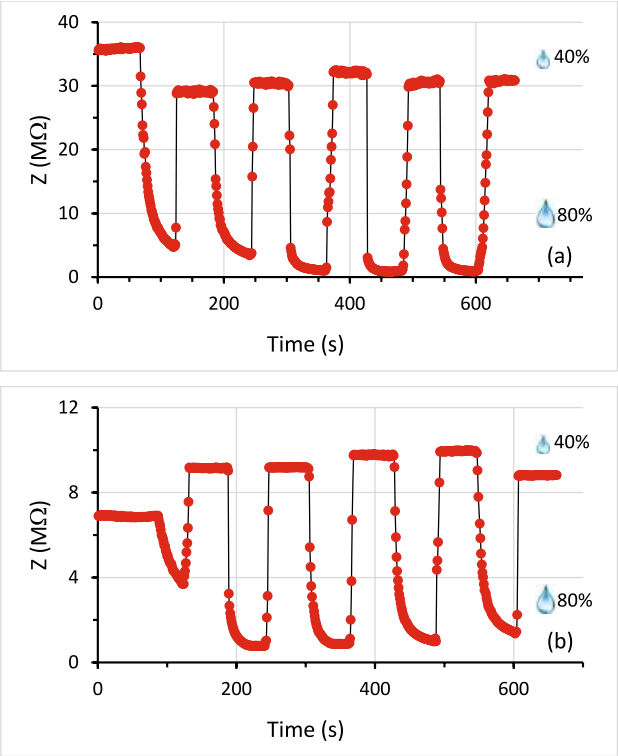

Fig. 17 Impedance switching cycles of $CaSO_4 \cdot 0.5H_2O$ samples obtained by isostatic pressing (IV) in the relative humidity range of 40–80% at a voltage of 1 V at frequencies of 200 Hz (**a**) and 1 kHz (**b**)

used for humidity sensors, which were analyzed in detail in Wang et al. (2013) and Tripathy et al. 2014).

For calcium sulfate hemihydrate—samples (I) and (IV), the response time and recovery time are comparable to other used humidity sensor materials.

To determine the sensitivity of the sample (IV) impedance to air humidity, formula (1) was used in the frequency range from 200 Hz to 1 MHz (Fig. 18). With increasing and decreasing humidity, hysteresis is observed, the nature of which changes depending on the signal frequency.

At a frequency of 200 Hz, the hysteresis loop has a closed shape over the entire range of relative humidity and a minimum area. With increasing frequency, the hysteresis loop increases its area and changes its shape, which correlates with a violation of cyclic reproducibility and the impedance value Z at high frequencies (Fig. 18). The study of the cyclicity of the impedance sensitivity of the $CaSO_4 \cdot 0.5H_2O$ sample to relative air humidity allows us to assume that it is necessary to increase the response time when changing the relative air humidity, which would allow using the sample (IV) as an air humidity sensor.

Table 5 Comparison of the parameters of humidity sensors made of calcium sulfate with the parameters of sensors based on tin oxide, titanium, zinc (Wang et al. 2013; Tripathy et al. 2014)

	Measuring range (%)	Response time (s)	Recovery time (s)	Hysteresis (%)
our samples				
sample (I), $f=1$ kHz	40–80	3	20	24
sample (II), $f=1$ kHz	40–80	6	13	11
sample (II), $f=200$ kHz	40–80	3	4	7
sample (III), $f=200$ Hz	40–80	10	11	7
sample (III), $f=1$ kHz	40–80	8	57	27
sample (IV), $f=200$ Hz	40–80	4	11	5
sample (IV), $f=1$ kHz	40–80	4	6	4
ZnO/GaN (Wang et al. 2013)				
ZnO/GaN	12–96	7	13	
several different types of humidity sensors (Tripathy et al. 2014)				
$CdTiO_3$ nanofibers		4	6	≈7
Develop a novel humidity sensor based on $Na_2Ti_3O_7$ nanowires		4	5	–
Pure TiO_2 and KCl-doped TiO_2 nano fibers with different crystallographic structures		3	3	–
Barium titanate ($BaTiO_3$) nanofiber		< 5	< 4	5
Electrospun TiO_2 nanofiber with metallic electrodes: titanium (Ti)		3	5	3
Electrospun TiO_2 nanofiber with metallic electrodes: nickel (Ni)		4	7	5
Electrospun TiO_2 nanofiber with metallic electrodes: gold (Au)		7	13	15
KCl-doped ZnO nanofibers		2	1	–
A-plane ZnO nanotip on R-plane sapphire substrate		3	12	1.9
KCl-doped SnO_2 nanofibers silver-paladium (Ag–Pd) interdigital electrodes substrate		5	6	–
KCl-doped nanoporous $Ti_{0.9}Sn_{0.1}O_2$ thin films		11	14	–
$ZnSnO_3$ cubic crystallites		7	6	–

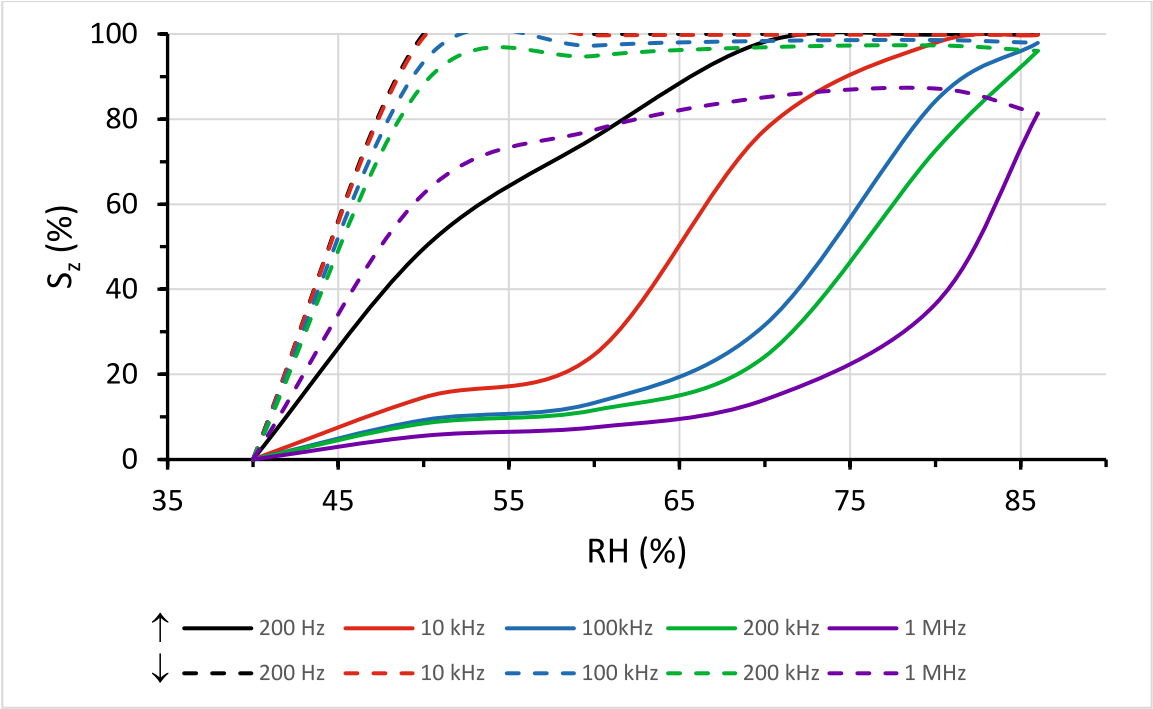

Fig. 18 Impedance sensitivity of $CaSO_4 \cdot 0.5H_2O$ samples obtained by isostatic pressing (IV) to humidity with increasing and decreasing humidity at frequencies of 200 Hz, 10 kHz, 100 kHz, 200 kHz, 1 MHz. The directions of the arrows show that the humidity in the test chamber increases (↑) or decreases (↓)

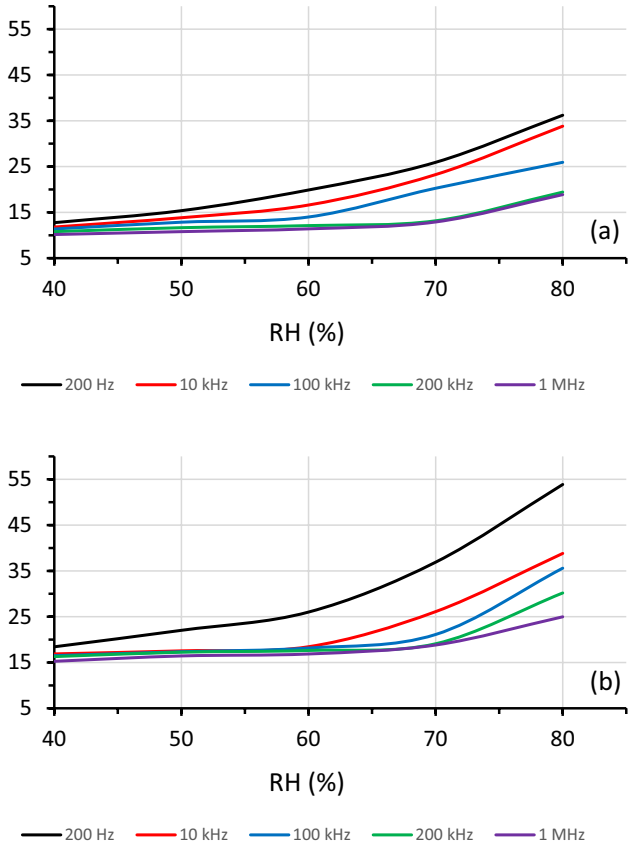

Fig. 19 Dependence of the relative permittivity, ε, on humidity for samples: (**a**) $CaSO_4 \cdot 0.5H_2O$ obtained by uniaxial pressing (II) and (**b**) $CaSO_4 \cdot 0.5H_2O$ obtained by isostatic pressing (IV) at frequencies of 200 Hz, 10 kHz, 100 kHz, 200 kHz, 1 MHz

Dependence of relative permittivity on humidity

We also investigated the dependence of the relative permittivity, ε, on humidity in the frequency range from 200 Hz to 1 MHz for samples (II) and (IV). For samples (I) and (III) made of $CaSO_4 \cdot 2H_2O$, the value of ε is close to the values of the relative permittivity for water (ε = 75 at T = 28 °C), which is due to the presence of crystalline water in the compound of calcium sulfate dihydrate and adsorption water taken from humid air.

The dependence of permittivity on frequency is called permittivity dispersion. As can be seen from Fig. 19, the pressing method affects the value of the relative permittivity, but does not affect its behavior.

For the samples made of calcium sulfate hemihydrate, ε depends on frequency, increases with increasing importance, and changes as follows. For the samples made by isostatic pressing, at a frequency of 200 Hz from 18 (at RH = 40%) to 54 (at RH = 80%), at a frequency of 1 MHz from 15 (at RH = 40%) to 25 (at RH = 80%). For the samples made by uniaxial pressing, the trend is preserved, but the values of the relative permittivity are somewhat lower: at a frequency of 200 Hz from 13 (at RH = 40%) to 36 (at RH = 80%), at a frequency of 1 MHz from 10 (at RH = 40%) to 19 (at RH = 80%).

Thus, all samples had the highest sensitivity at a frequency of 200 Hz, with an increase in frequency, the relative permittivity decreases for samples (II) and (IV), and at the same time, the sensitivity to humidity worsens.

This dispersion of the relative permittivity, expressed in a monotonic decrease in the relative permittivity with increasing frequency, is called relaxation. It is characteristic of the dipole and migration mechanisms of polarization (Barsoukov 2018).

Conclusion

The sensitivity of calcium sulfate hemihydrate $CaSO_4 \cdot 0.5H_2O$ and calcium sulfate dihydrate $CaSO_4 \cdot 2H_2O$ samples to air humidity was studied using impedance spectroscopy depending on the pressing method: uniaxial, using Universal Testing Machine (Instron Electromechanical Testing systems) Model 3369 and cold isostatic, using an EPSI isostatic press. The frequency dependences of the complex resistance on relative humidity, impedance switching cycles were measured during sequential movement of samples from a test chamber with a relative air humidity of 80% to a reference chamber with a relative air humidity of 40% at frequencies from 200 Hz to 1 MHz. It was found that for samples (II–IV) hodographs are observed in the entire range of air humidity (Figs. 7, 11, 15), for samples (I) the hodograph is observed only at RH = 40% before testing in a humid environment. When the humidity decreases to RH = 40% without preliminary drying of the sample, the hodograph is not restored. Based on the results of studies of cyclic switching of the impedance of samples in the range at RH = 40–80% at a frequency of 200 Hz on samples (III) and (IV), the possibility of their practical application as a new material for an air humidity sensor is shown. The dependence of relative permittivity on humidity in the frequency range from 200 Hz to 1 MHz for samples (II) and (IV) was studied. It was shown that the value of relative permittivity is affected by the pressing method. A monotonic decrease in relative permittivity with increasing frequency is observed. The experimentally established presence of impedance switching cycles (Figs. 13, 16) samples of calcium sulfate hemihydrate $CaSO_4 \cdot 0.5H_2O$ and calcium sulfate dihydrate

$CaSO_4 \cdot 2H_2O$ were obtained from industrial waste, citrogypsum, with changes in relative air humidity in the range of 40–80% indicates the possibility of using these materials in the production of air humidity sensors. To study reproducibility and repeatability, the experiments lasted for a month and in between experiments the samples were stored natural conditions. When studying the electrical characteristics, the standard deviation of the response time in the cyclic dependencies of the complex resistance of materials was within 3σ.

Thus, we propose a new method for using industrial waste associated with obtaining the main component of the air humidity sensor—a moisture-absorbing layer made of citrogypsum. This method will also help to preserve the environment and resources, as well as reduce the burden on waste storage facilities, thereby closing the cycle of a sustainable economy.

Acknowledgements This work was supported by the Ministry of Science and Higher Education of the Russian Federation under the State Assignment for the creation of new laboratories, including under the guidance of young promising researchers of the national project "Science and Universities". The research title is "Elaboration and development of scientific and technological foundations for creating an integrated technology for processing gypsum-containing waste from various industrial enterprises and searching of new ways to use processed products" (Grant number FZWG-2024-0001).

Declarations

Conflict of interest The author has no competing interests to declare.

References

Abe Y, Nishizaki S, Muroi T, Kato Y, Hench LL (2006) Conversion of gypsum into a superprotonic conductor. Mater Res Innov 10:93. https://doi.org/10.1179/mri.2006.10.1.93

Abe Y, Yoshikawa D, Ito M, Taguchi H (2007) Superprotonic conductors of gypsums containing H_3PO_4 for fuel cells below 200 °C. Electrochem Solid-State Lett 10:B111. https://doi.org/10.1149/1.2737543

Adhikari AB, Majumdar S (2004) Influence of molecular architecture on morphology and micromechanical behavior of styrene/butadiene block copolymer systems. Progr Polym Sci 29(7):699–766. https://doi.org/10.1016/j.progpolymsci.2004.06.002

Alfimova NI, Pirieva SY, Elistratkin MY, Nikulin IS, Titenko AA (2020) Binders from gypsum-containing waste and products based on them. IOP Conf Ser Mater Sci Eng 945(1):012057. https://doi.org/10.1088/1757-899X/945/1/012057

Barsoukov E (2018) Impedance spectroscopy: theory, experiment, and applications. In: Barsoukov E, Macdonald JR (eds) Fundamentals of impedance spectroscopy. Wiley, Hoboken, p 606. https://doi.org/10.1002/9781119381860

Bridgeman D, Corral J, Quach A, Xian X, Forzani E (2014) Colorimetric humidity sensor based on liquid composite materials for the monitoring of food and pharmaceuticals. Langmuir 30(35):10785–10791. https://doi.org/10.1021/la502593g

Gu K, Chen B (2020) Loess stabilization using cement, waste phosphogypsum, fly ash and quicklime for self-compacting rammed earth construction. Constr Build Mater 231:117195. https://doi.org/10.1016/j.conbuildmat.2019.117195

Hossein-Babaei F, Shabani P (2014) A gold/organic semiconductor diode for Ppm-level humidity sensing. Sens Actuators B Chem 205:143–150. https://doi.org/10.1016/j.snb.2014.08.061

Huang Y, Qian J, Lu L, Zhang W, Wang S, Wang W, Cheng X (2019) Phosphogypsum as a component of calcium sulfoaluminate cement: Hazardous elements immobilization, radioactivity and performances. J Clean Prod 248:119287. https://doi.org/10.1016/j.jclepro.2019.119287

Kang U, Wise KD (2000) A high-speed capacitive humidity sensor with on-chip thermal reset. IEEE Trans Electron Devices 47(4):702–710. https://doi.org/10.1109/16.830983

Li Y, Yang MJ (2002) Humidity sensitive properties of a novel soluble conjugated copolymer: ethynylbenzene-co-propargyl alcohol. Sens Actuators B Chem 85(1–2):73–78. https://doi.org/10.1016/S0925-4005(02)00055-2

Matko V, Donlagic D (1996) Sensor for high-air-humidity measurement. IEEE Trans Instrum Meas 45(2):561–563. https://doi.org/10.1109/19.492787

Nikulicheva TB, Zakhvalinsky VS, Pilyuk EA, Nikulin IS, Vyazmin VV, Mishunin MV, Saenko MY, Telpova OA, Alfimova NI, Erina TA (2023a) Properties of citrogypsum and possibilities of its application in technology. J Tech Phys 93(9):1320–1328. https://doi.org/10.21883/JTF.2023.09.56219.113-23. (**In Russian**)

Nikulicheva TB, Zakhvalinskii VS, Pilyuk EA, Nikulin IS, Vyazmin VV, Mishunin MV (2023b) New humidity sensor material $(CaSO_4 \cdot 2H_2O)_{0.975}$–$(CuSO_4 \cdot 5H_2O)_{0.025}$. Materialia 27:101662. https://doi.org/10.1016/j.mtla.2022.101662

Nikulicheva TB, Zakhvalinskii VS, Pilyuk EA, Nikulin IS, Vyazmin VV, Mishunin MV, Saenko MY, Telpova OA, Alfimova NI, Erina TA (2024) The possibility of practical application of citrogypsum in engineering. Tech Phys 69(5):1307–1315. https://doi.org/10.1134/S1063784224040297

Patrusheva TN, Barashkov VA, Churbakova OV, Petrov SK (2018) Ecological problems of electronic means production and utilization. J Siber Feder Univ Eng Technol 11(6):679–693. https://doi.org/10.17516/1999-494X-0085

Selyanchyn R, Wakamatsu S, Hayashi K, Lee SW (2015) A nano-thin film-based prototype QCM sensor array for monitoring human breath and respiratory patterns. Sensors 15(8):18834–18850. https://doi.org/10.3390/s150818834

Sirimahasal T, Kalhong Y, Simasatitkul L, Pranee S, Seeyangnok S (2019) The effect of solvent polarity on phase transformation of Citrogypsum via hydrothermal process. Key Eng Mater 803:351–355. https://doi.org/10.4028/www.scientific.net/KEM.803.351

Suzuki S, Katagiri Y, Nagai M (2011) Intermediate temperature fuel cell using gypsum based electrolyte and electrodes. IOP Conf Ser Mater Sci Eng 18:122008. https://doi.org/10.1088/1757-899X/18/12/122008

Tao X, Liao S, Wang Y (2021) Polymer-assisted fully recyclable flexible sensors. EcoMat 3(2):e12083. https://doi.org/10.1002/eom2.12083

Tripathy A, Pramanik S, Cho J, Santhosh J, Abu Osman NA (2014) Role of morphological structure, doping, and coating of different materials in the sensing characteristics of humidity sensors. Sensors 14:16343–16422. https://doi.org/10.3390/s140916343

Vooka P, George B (2014) A direct digital readout circuit for impedance sensors. IEEE Trans Instrum Meas 64(4):902–912. https://doi.org/10.1109/TIM.2014.2361552

Wang K, Qian X, Zhang L, Li Y, Liu H (2013) Inorganic–organic p–n heterojunction nanotree arrays for a high-sensitivity diode

humidity sensor. ACS Appl Mater Interfaces 5(12):5825–5831. https://doi.org/10.1021/am4014677

Xin Y, Xiang L, Yu YX (2015) Influence of structure on the morphology of $CaSO_4 \cdot nH_2O$ ($n = 0, 0.5, 2$): a molecular simulation study. Mater Res Innov 19(sup2):S2-103-S2-107. https://doi.org/10.1179/1432891715Z.0000000001313